08,13,14

Study of crystal fragmentation under all-round compression

© M.N. Magomedov

Institute for Problems of Geothermy and Renewable Energy — branch of the Joint Institute for High Temperatures of RAS,
Makhachkala, Dagestan, Russia

E-mail: mahmag4@mail.ru

Received November 21, 2024
Revised January 13, 2025
Accepted January 14, 2025

We studied the variation of the specific (per unit area) surface energy (σ) of a crystal from the normalized volume (v/v_0) along the different isotherms based on the analytical method (i.e., without computer modeling). Here, v_0 is the volume value at zero values of pressure and Kelvin temperature. It is shown that the function $\sigma(v/v_0)$ under a certain compression $(v/v_0)_{\text{frS}} < 1$ passes into the negative value region. This behavior of the $\sigma(v/v_0)$ function at $v/v_0 < (v/v_0)_{\text{frS}}$ should stimulate crystal fragmentation, in which the crystal will seek to increase its intercrystalline surface in any way. It is shown that the negative value of the function $\sigma(v/v_0)$ should stimulate both the fragmentation of the crystal structure and the heating of the fragmenting medium and the appearance of surface pressure in this medium due to the appearance of the inner surface. Calculations of the $(v/v_0)_{\text{frS}}$ value for Ne, Li and Au crystals at different temperatures have been carried out. Based on the experimental data, the pressures were indicated, which correspond to the calculated $(v/v_0)_{\text{frS}}$ values. It was shown that these pressures are quite achievable in modern experiments on the static compression of these crystals.

Keywords: deformation, surface energy, nanocrystal, surface pressure.

DOI: 10.61011/PSS.2025.02.60685.318

1. Introduction

Crystal fragmentation in all-round compression is defined as transformation of a single crystal into a nanocrystal system at hydrostatic pressure. This work is devoted to the study of this effect. Comprehensive study of substance properties at high pressures is currently underway. Static pressures may reach $1\,\text{TPa} = 1000\,\text{GPa} = 10\,\text{Mbar}$ [1]. However, the baric fragmentation effect, where the single crystal structure is transformed into a disoriented domain system, is not taken into account. Domain is a crystal region that differs from the neighboring regions in the shift vector direction and has an interdomain surface. The baric fragmentation effect in all-round (hydrostatic) compression of a single crystal was first noted by P.W. Bridgman, who wrote: „It is conceivable that the crystal might be broken up into a mosaic of smaller and smaller blocks, with little alteration of structure within the block . . .“ [2, p. 286]. Meanwhile, the baric fragmentation effect in crystal compression above a particular pressure has been already discovered [3–6], whereby the domain size may reach a nanolevel during the baric fragmentation [5,6].

However, the nature of baric fragmentation is not clear and none of the existing methods for calculating substance properties in extreme compressions takes into account the baric fragmentation effect. It is assumed in this field of science that occurrence of internal surfaces in a crystal under pressure doesn't make any significant contribution to the crystal properties. However, it can be easily understood that crystal fragmentation shall contribute both to alteration of structure and to energy and system equation of state. In this regard, the following questions arise:

1. Why does the crystal fragment into domains in all-round compression, with an increase in its internal interdomain surface?

2. How does the temperature affect the baric fragmentation process in a crystal?

3. How does the medium pressure vary in transition from single-crystal to nanodispersed state?

The baric fragmentation process has been very little studied theoretically, by either analytical or computer simulation methods. Therefore, the literature doesn't give answers to the above questions. Moreover, as noted in [6], „the classical dislocational and disclinational approaches, successfully used earlier to describe ordinary macroscopic deformations, turned out to be insufficient in this case“. It is obvious that to answer the set questions, the dependence of the specific (per unit area) surface energy (σ) both on the specific (per atom) volume ($v = V/N$) and temperature (T) of the crystal and on the number of atoms (N) in the domain shall be known. Unfortunately, experimental measurement of σ for the solid phase is a very labor-consuming procedure that can be implemented at atmospheric pressure only at high temperatures [7–9]. Therefore, much attention is being paid to theoretical prediction of function $\sigma(v, T)$ both for macrocrystals and nanocrystals. However, the dependence of $\sigma(v, T, N)$ turned out to be very difficult to determine using either analytical or computer simulation methods [10]. Therefore, the literature so far gives no answer to the question about the baric dependence of σ even for a

macrocrystal. So, the above-mentioned questions are still unanswered.

This study proposes one of the possible answer options. An analytical method (i.e. without computer simulation) based on a nanocrystal model in the form of a rectangular parallelepiped (RP), the shape of which may be varied using a shape parameter. This method was called the RP model in [10–14]. To date, only this analytical method allows the baric dependence of σ to be studied at various temperatures both for macrocrystal and nanocrystal with a particular surface shape.

2. Calculation method

The RP model method, fundamentals of which were first described in [11] and further developed in [10,12–14], is used to calculate the dependence of the specific surface energy of a nanocrystal consisting of N atoms on arguments v and T. The RP model implies that a nanocrystal with the Gibbs free surface is a rectangular parallelepiped with a square base, the shape of which may be varied using a shape parameter: $f = N_{ps}/N_{po}$. Here, N_{ps} is the number of atoms on a side edge, N_{po} is the number of atoms on the edge of the square base of square parallelepiped. For a rod-like shape $f > 1$, for a cube $f = 1$, for a plate-shaped nanocrystal $f < 1$.

The pair interatomic interaction will be given by the Mie–Lennard-Jones potential written as

$$\phi(r) = \frac{D}{(b-a)}\left[a\left(\frac{r_0}{r}\right)^b - b\left(\frac{r_0}{r}\right)^a\right], \quad (1)$$

where D and r_0 are the depth and coordinate of the potential minimum, $b > a > 1$ are numerical variables, r is the distance between atom centers.

When using the „only nearest-neighbor interaction“ approximation within the RP model for the specific surface energy of nanocrystal facet (100), the following expression was obtained [12–14]

$$\sigma(N, f) = -\frac{k_n(\infty)DR^2}{12\alpha^{2/3}r_0^2}\left[U(R) + 3H_w(N, T)\right]. \quad (2)$$

Here, $R = r_0/c$ is the relative linear density of crystal, $c = (6k_p v/\pi)^{1/3}$ is the mean (with respect to nanosystem volume) distance between the nearest atom centers, k_p is the packing index of a structure consisting of N atoms, $k_n(\infty) = k_n(N = \infty)$ is the coordination number for a macrocrystal, $\alpha = \pi/(6k_p)$ is the structure parameter.

Functions introduced in (2) are written as:

$$U(R) = \frac{aR^b - bR^a}{b-a}, \quad (3)$$

$$H_w(N, T) = \frac{6\gamma(N, f)}{(b+2)}\left[\frac{k_B\Theta_E(N, f)}{Dk_n(N, f)}\right]E_w\left(\frac{\Theta_E}{T}\right), \quad (4)$$

$$E_w(y) = 0.5 + \frac{1}{[\exp(y) - 1]}, \quad (5)$$

$$k_n^* = \frac{k_n(N, f)}{k_n(\infty)} = 1 - Z_s(f)\left(\frac{\alpha^2}{N}\right)^{1/3}, \quad (6)$$

$$Z_s(f) = \frac{1 + 2f}{3f^{2/3}}. \quad (7)$$

Here, $k_n(N, f)$ is the mean (with respect to the whole nanosystem) first coordination number, k_B is the Boltzmann constant, $\Theta_E = (3/4)\Theta$ is the Einstein temperature, Θ is the Debye temperature, γ is the first Gruneisen parameter.

For Θ and γ, when using the „only nearest-neighbor interaction“ approximation, the following equations were derived [15,16]:

$$\Theta(k_n, c) = A_w(k_n, c)\xi\left[-1 + \left(1 + \frac{8D}{k_B A_w(k_n, c)\xi^2}\right)^{1/2}\right], \quad (8)$$

$$\gamma = -\left(\frac{\partial \ln\Theta}{\partial \ln v}\right)_T = \frac{b+2}{6(1+X_w)}, \quad (9)$$

$$X_w = \frac{\xi A_w}{\Theta}. \quad (10)$$

The following notations are introduced here:

$$A_w(k_n, c) = K_R\,\frac{5k_n\,ab(b+1)}{144(b-a)}\left(\frac{r_0}{c}\right)^{b+2}, \quad (11)$$

$$K_R = \frac{\hbar^2}{k_B r_0^2 m}, \quad \xi = \frac{9}{k_n(\infty)}, \quad (12)$$

where $\hbar$ is the Planck constant, m is the atomic mass.

Note that, when deriving expressions (8)–(12), it was assumed that Θ remains unchanged during isochoric heating. Otherwise, expressions for Θ and γ will take a more complex form [15,16].

With a finite number of atoms in the nanocrystal, surface pressure P_{sf} occurs and is equal to [10,12,14] within the RP model

$$P_{sf}(T, v, N, f) = \left[\frac{\partial(\sigma\Sigma/N)}{\partial v}\right]_{T,N} = P_{Ls}(1 - \Delta_p). \quad (13)$$

The first term in (13) is the Laplace pressure that is defined by the change of surface area (Σ) variation with the change of nanocrystal volume:

$$P_{Ls}(T, v, N, f) = \sigma\left[\frac{\partial(\Sigma/N)}{\partial v}\right]_{T,N} = \frac{4\alpha^{1/3}Z_s(f)}{N^{1/3}c}\,\sigma = 4\,\frac{(1 - k_n^*)}{\alpha^{1/3}c}\,\sigma. \quad (14)$$

Expression for Δ_p from equation (13) is written as

$$\Delta_p = -\left[\frac{\partial \ln(\sigma)}{\partial \ln(\Sigma/N)}\right]_{T,N} = -\frac{1}{2}\left[\frac{\partial \ln(\sigma)}{\partial \ln(c)}\right]_{T,N,k_p,f} = 1 + \frac{1}{2L_E(N, f)}\left\{U'(R) - 9\left[q - \gamma t_y\left(\frac{\Theta_E}{T}\right)\right]H_w(N, T)\right\}. \quad (15)$$

In (15), the second Gruneisen parameter (q) and the introduced functions are written as:

$$\left.\begin{aligned} q&=\left(\frac{\partial \ln\gamma}{\partial \ln v}\right)_T=\gamma\,\frac{X_w(1+2X_w)}{(1+X_w)}=\frac{(b+2)X_w(1+2X_w)}{6(1+X_w)^2},\\ L_E(N,\,f)&=U(R)+3H_w(N,\,T),\\ U'(R)&=R\left[\frac{\partial U(R)}{\partial R}\right]=\frac{ab(R^b-R^a)}{b-a},\\ t_y(y)&=\frac{\partial \ln[yE_w(y)]}{\partial \ln y}=1+\frac{\partial \ln[E_w(y)]}{\partial \ln y}=1-\frac{2y\exp(y)}{[\exp(2y)-1]} \end{aligned}\right\}. \tag{16}$$

In the „thermodynamic limit“ (i.e. when $N\to\infty$ and $V\to\infty$ at $v=V/N=\text{const}$) from (6), we obtain $k_n^*(N\to\infty)\to 1$. Then the expressions from (2), (4), (8)–(11), (15) and (16) are rearranged to equations for a macrocrystal, and P_{sf} from (13) and P_{Ls} from (14) vanish.

Equation (2) was tested for various substances in different $P-T$-conditions, from 0 K to the melting temperature (T_m). With $P\cong 0$, a good agreement with experimental estimates was achieved for many elementary crystals with various structures, with different types of chemical bond and different roles of quantum effects [11–14,17–21]. At low pressures and room temperatures, i.e. at $R=r_0/c\cong 1$ and $T\cong\Theta_E$, we have $U(R\cong 1)\cong -1$, $E_w(y\cong 1)\cong 1$. Hence, for the „classical“ substance (i.e. at $k_nD/(k_B\Theta_E)\gg 1$), we have

$$\sigma(R\simeq 1,\,T\simeq\Theta)\simeq\frac{k_n(\infty)D}{12\alpha^{2/3}r_0^2}>0. \tag{17}$$

Let's study the change of surface energy and surface pressure functions in extreme all-round compression of the crystal along various isotherms.

As shown by equations (2)–(16), in ultimate all-round compression (i.e. with $v/v_0=(c/r_0)^3\to 0$, or with $R=r_0/c\to\infty$), the following relations are satisfied [12,14]

$$\lim_{v/v_0\to 0}\sigma=-\frac{k_n(\infty)Da}{12\alpha^{2/3}r_0^2(b-a)}\lim_{R\to\infty}R^{b+2}=-\infty, \tag{18}$$

$$\lim_{v/v_0\to 0}P_{\text{Ls}}=-\frac{Z_s(f)}{N^{1/3}}\,\frac{k_n(\infty)Da}{3\alpha^{1/3}r_0^3(b-a)}\lim_{R\to\infty}R^{b+3}=-\infty, \tag{19}$$

$$\lim_{v/v_0\to 0}P_{\text{sf}}=\frac{Z_s(f)}{N^{1/3}}\,\frac{k_n(\infty)Dab}{6\alpha^{1/3}r_0^3(b-a)}\lim_{R\to\infty}R^{b+3}=\infty. \tag{20}$$

Here, $v=\pi c^3/(6k_p)$ and $v_0=\pi r_0^3/(6k_p)$ are specific (per atom) volumes with the distance between the centers of nearest atoms equal to $c(P,\,T)$ and r_0, respectively. Thus, v/v_0 is the ratio of the specific volume with P and T to the specific volume with $P=0$ and $T=0$ K.

Equations (2)–(16) also show that, in ultimate all-round stretching (i.e. with $v/v_0\to\infty$, or with $R\to 0$), the following relations are satisfied

$$\lim_{v/v_0\to\infty}\sigma=-\frac{k_BT}{4\alpha^{2/3}r_0^2k_n^*}\lim_{R\to 0}R^2=-0, \tag{21}$$

$$\lim_{v/v_0\to\infty}P_{\text{Ls}}=-\frac{Z_s(f)}{N^{1/3}}\,\frac{k_BT}{\alpha^{1/3}r_0^3k_n^*}\lim_{R\to 0}R^3=-0, \tag{22}$$

$$\lim_{v/v_0\to\infty}P_{\text{sf}}=-\frac{Z_s(f)}{N^{1/3}}\,\frac{k_n(\infty)D(b+2)}{4\alpha^{1/3}r_0^3}\times\lim_{R\to 0}\left[X_w-\frac{1}{6}\left(\frac{\Theta_E}{T}\right)^2\right]H_w(N,\,T)R^3=-0. \tag{23}$$

Thus, it follows from (18) and (21) that the surface energy of the crystal becomes negative in compression of the crystal volume below a certain level (i.e. with $v/v_0<(v/v_0)_{\text{frS}}<1$) or in all-round stretching above a certain value (i.e. with $v/v_0>(v/v_0)_{\text{frL}}>1$). Such behavior of $\sigma(P)$ in compression along the isotherm $T=0$ K was also indicated in [22]. There are no any thermodynamic principles prohibiting negative surface energies, as it was shown in [23–25].

In case when the all-round stretching is higher than a certain value (i.e. with $v/v_0>(v/v_0)_{\text{frL}}>1$), appearance of cracks and future crystal fracture was understood physically [26,27]. This also follows from (21). However, it was not clear: why do cracks and domains occur in all-round (hydrostatic) compression? It is obvious that fluctuations in a thermodynamically-equilibrium single crystal shall decrease as the all-round pressure grows. From these considerations, it would seem that the single crystal structure in compression should become more uniform. The crystal becomes denser and it would seem that there should be no cracks and domains. However, according to the experiments [3–6,28], this is the case only with relatively low degrees of all-round compression (with $v/v_0>0.85$), but in higher compressions (with $v/v_0<0.6$), the single crystal structure of a monoatomic substance changes to a mosaic domain structure. This effect can be easily explained, if the result from (18) is taken into account.

From expression (2), it can be also seen that there is such „fragmentation temperature“: $T_{\text{fr}}\gg\Theta_E(v/v_0)$, above which the crystal surface energy was negative at any pressure. I.e. when $T\geq T_{\text{fr}}$, then with any v/v_0, $\sigma(v/v_0,\,T\geq T_{\text{fr}})\leq 0$ will be satisfied. From (2), an expression for the „fragmentation temperature“ can be easily derived and is written as [11]

$$T_{\text{fr}}(N,\,f)=\frac{(b+2)Dk_n(N,\,f)}{18(b-a)k_B}\max\left[\frac{bR^a-aR^b}{\gamma(R)}\right]\approx\frac{k_n(N,\,f)D}{3k_B}. \tag{24}$$

As shown by (24), the following relation is satisfied

$$T_{\text{fr}}(N)<T_{\text{fr}}(N=\infty)<\Theta_{\max},$$

where

$$\Theta_{\max}=\lim_{v/v_0\to 0}\Theta=\frac{4k_n(\infty)D}{9k_B}. \tag{25}$$

It is easy to understand that with $\sigma<0$ fragmentation shall start: the crystal will tend to increase its specific (per

atom) surface in any way: either free surface (in tension), or intercrystalline surface (in compression). Therefore, „non-cubic“ (rod-like, flat or tree-like) forms will be more energetically favorable for domains that are formed during fragmentation than cubic forms that are energetically favorable with $v/v_0 > (v/v_0)_{\text{frS}}$.

Calculations showed [25] that a degree of all-round stretching, at which the specific surface energy moves to a negative region $(v/v_0)_{\text{frL}}$, lies in a liquid phase or gas phase region for all examined substances (inert gas crystals, iron, diamond, silicon, and germanium). Therefore, the crystal in all-round stretching changes to a liquid or gas phase without reaching a negative surface energy value.

However, a negative surface energy may be reached in uniform compression of the crystal. The energy Q related to formation of the surface area Σ will be released during transition from the single-crystal state, which is unstable with $v/v_0 \le (v/v_0)_{\text{frS}} < 1$, to a more energetically favorable (due to $\sigma < 0$) nanostructured state. The smaller the „average“ domain size achieved as a result of fragmentation of a single crystal the higher the energy, as shown in [23–25]. Specific (per unit volume) energy related to formation of the surface area Σ is equal to

$$\frac{Q}{V} = \frac{1}{V}\iint\limits_{\Sigma} \sigma(\Sigma)d\Sigma \simeq \frac{\Sigma}{V}\sigma. \tag{26}$$

If $\sigma > 0$, then $Q > 0$. Energy is absorbed during this process, i.e. this is the endothermic process. During fragmentation $\sigma < 0$, and therefore $Q < 0$, i.e. energy is released in this case, and this is an exothermic process.

Assume that during fragmentation a single crystal is broken up into N_{F} identical „average“ nanocrystals with size N_m, shape parameter f_m, volume $V_1(N_m)$ and surface area $\Sigma_1(N_m, f_m)$. Volume and surface area of such system are $V = N_{\text{F}}V_1(N_m)$ and $\Sigma = N_{\text{F}}\Sigma_1(N_m, f_m)$, respectively. Then, according to the mean value theorem for integrals, equation (26) may be written as

$$\frac{Q}{V} = \frac{\Sigma_1(N_m, f_m)}{V_1(N_m)}\sigma(N_m, f_m). \tag{27}$$

Within the RP model, the following expressions were derived for the volume and surface area of a nanocrystal consisting of N_m atoms [10–14]

$$V_1(N_m) = N_m v = \alpha c^3 N_m,$$

$$\Sigma_1(N_m, f_m) = 6c^2\alpha_s(\alpha N_m)^{2/3}Z_s(f).$$

Then equation (27) may be rearranged to the following form:

$$\frac{Q}{V} = \frac{6\alpha_s Z_s(f_m)}{c(\alpha N_m)^{1/3}}\sigma(N_m, f_m) = \frac{6\alpha^{1/3}Z_s(f_m)}{cN_m^{1/3}}\sigma(N_m, f_m). \tag{28}$$

From (28), it can be seen that the specific heat increases as the „average“ nanocrystal size decreases and as its shape differs more significantly from the energetically optimum shape at $v/v_0 > (v/v_0)_{\text{frS}}$ (this is cube for the RP model). Note also that the intercrystalline surface energy of the domain (σ_d) in a nanostructured solid body is related to the surface energy of a nanocrystal with free surface as follows [29]: $\sigma_d = \chi\sigma(100)$, where coefficient χ depends on the indices of contacting domain facets: $1 > \chi > 0$.

As shown by (20), in the baric fragmentation region, i.e. with $v/v_0 < (v/v_0)_{\text{frS}} < 1$, the surface pressure may play a significant role both for an individual nanocrystal and for the whole nanostructured medium. The formed domains undergo additional all-round compression that increases as the domain size decreases and as the domain shape differs more significantly from the energetically optimum shape with $v/v_0 > (v/v_0)_{\text{frS}}$ (this is cube for the RP model). The higher the external pressure the lower the dependence of P_{Ls} and P_{sf} on temperature and the higher P_{sf}. As shown in [10–14,17–21], additional all-round pressure P_{sf} will cause a decrease in the compression modulus $(B_T = -v(\partial P/\partial v)_T)$ both for an individual nanocrystal and for the whole nanostructured medium. This is due to the fact that the nanostructured medium will be compressed more at the same external pressure P than the macrocrystal (due to $P + P_{\text{sf}}$).

3. Calculation results

Three crystals with various structures and properties were taken for calculations. Ne and Au have a face-centered cubic (FCC) structure: $k_n(\infty) = 12$, $k_p = 0.7405$. Li has a body-centered cubic (BCC) structure: $k_n(\infty) = 8$, $k_p = 0.6802$. Table 1 shows potential (1) parameters for Ne, Li, Au and references to the papers where they were determined and tested.

Molar volumes derived from them with $c = r_0$: $v_0 = \pi r_0^3/(6k_p)$, Debye temperatures from (8) and Gruneisen parameters from (9) and (16) for macrocrystals with $v/v_0 = 1$ are shown in other columns. Macrocrystal fragmentation temperatures $T_{\text{fr}}(\infty)$ were calculated using equation (24), and $\Theta_{\max}$ was calculated using equation (25). Bottom lines for $\Theta(1)$ and $\gamma(1)$ show the experimental values for macrocrystals with $T = 0\,\text{K}$ and $P = 0$ from [30–33].

Surface properties were calculated both for the macrocrystal $(N = \infty)$ and for the cubic nanocrystal $(f = 1)$ with the number of atoms on the edge equal to $N_{\text{po}} = 6$. Thus, the number of atoms for the FCC nanocrystal is $N(\text{FCC}) = (6k_p/\pi)fN_{\text{po}}^3 = 306$ and for the BCC nanocrystal is $N(\text{BCC}) = 281$. Calculations were performed for three temperatures: both below and above the macrocrystal melting temperature T_m at $P = 0$.

Figures 1–3, *a* shows isothermal dependences of the specific surface energy (in $10^{-3}\,\text{J/m}^2$) of the (100) facet on the normalized volume: $v/v_0 = (c/r_0)^3$, calculated using equation (2) for the specified crystals. Solid curves — calculated data for the macrocrystal, dashed lines — calculated data for the cubic nanocrystal $(f = 1)$ with

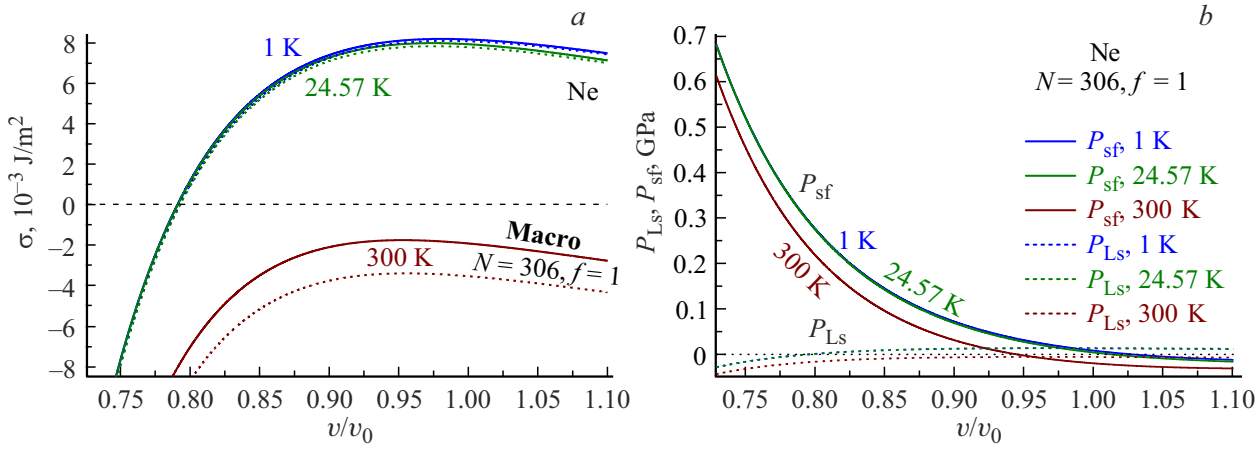

Figure 1. Isothermal dependences of the surface properties on the normalized volume for FCC-Ne. *a*) Isotherms $\sigma(\upsilon/\upsilon_0)$: solid lines — for the macrocrystal, dashed lines — for the nanocrystal consisting of 306 atoms. *b*) Isotherms for P_{sf} (solid lines) and for P_{Ls} (dashed lines) calculated for the nanocrystal consisting of 306 atoms.

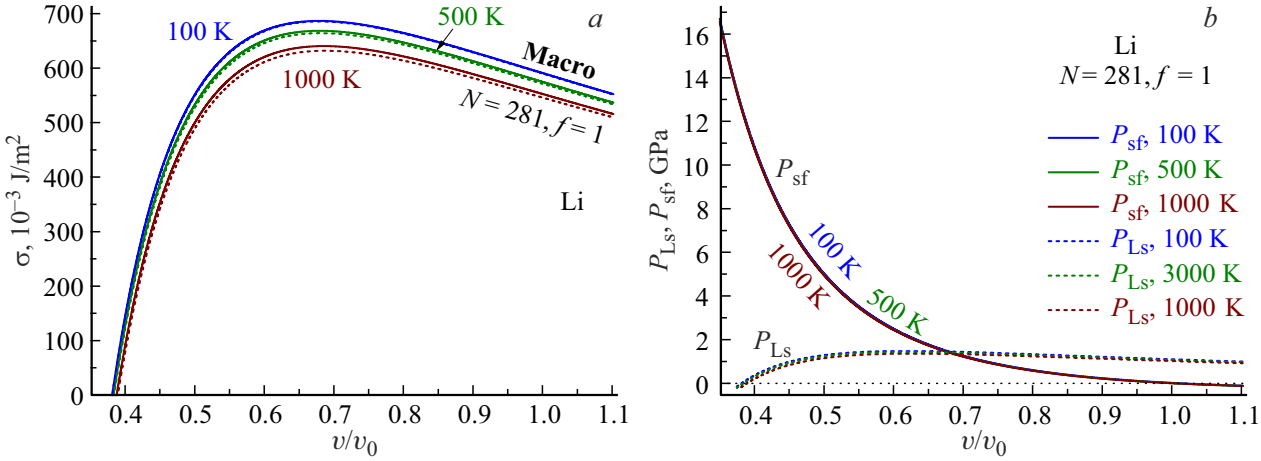

Figure 2. Isothermal dependences of the surface properties on the normalized volume for BCC-Li. *a*) Isotherms $\sigma(\upsilon/\upsilon_0)$: solid lines — for the macrocrystal, dashed lines — for the nanocrystal consisting of 281 atoms. *b*) Isotherms for P_{sf} (solid lines) and for P_{Ls} (dashed lines) calculated for the nanocrystal consisting of 281 atoms.

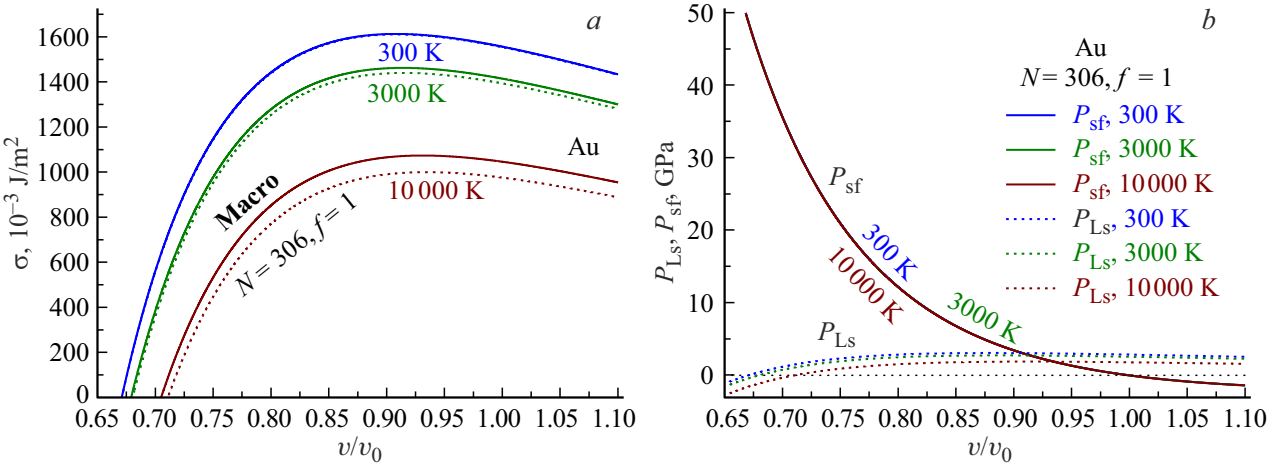

Figure 3. Isothermal dependences of the surface properties on the normalized volume for FCC-Au. *a*) Isotherms $\sigma(\upsilon/\upsilon_0)$: solid lines — for the macrocrystal, dashed lines — for the nanocrystal consisting of 306 atoms. *b*) Isotherms for P_{sf} (solid lines) and for P_{Ls} (dashed lines) calculated for the nanocrystal consisting of 306 atoms.

Table 1. Potential (1) parameters and the values of Debye temperature and Grüneisen parameters at $v/v_0 = 1$ as well as of $T_{fr}(\infty)$ and Θ_{max} derived from them for the macrocrystal

Crystal m, amu	r_0, 10^{-10} m	D/k_B, K	b	a	Ref.	v_0, cm^3/mol	$\Theta(1)$, K	$\gamma(1)$	$q(1)$	$T_{fr}(\infty)$, K	Θ_{max}, K
FCC-Ne 20.18	3.1563	52.59	21.39	5.83	[30,31]	13.3893	74.635 63−75	3.30 2.6−3.5	0.690	210.36	280.48
BCC-Li 6.941	3.0077	4930.10	5.15	1.65	[30,32]	12.6129	351.91 344−448	1.18 0.89−1.18	0.012	13146.93	17529.24
FCC-Au 196.967	2.8700	7446.04	15.75	2.79	[13,33]	10.0663	204.765 162−190	2.951 2.3−3.38	0.008	29784.16	39712.20

the number of atoms on the edge $N_{po} = 6$, i.e. $N = 306$ for FCC-Ne and FCC-Au crystals, $N = 281$ for BCC-Li crystal. Figures 1−3, *b* shows (in GPa) dependences of the surface pressure P_{sf} from (13) and the Laplace pressure P_{Ls} from (14) on the normalized volume: v/v_0, calculated for the cubic nanocrystal ($f = 1$) with the number of atoms on the edge $N_{po} = 6$. Solid lines — calculated data for P_{sf}, dashed lines — calculated data for P_{Ls}.

Figure 1 from top to bottom shows isotherms $T = 1$, 24.57, 300 K for FCC-Ne ($T_m(P = 0) = 24.57$ K). Figure 1, *a* shows that the dependence of the specific surface energy $\sigma(v/v_0)$ along isotherm $T = 300$ K lies below zero at any v/v_0. I.e. the Ne crystal at this temperature tends to increase its surface at any pressure. As shown in Figure 1, *b*, for the nanocrystal consisting of 306 atoms, dependences for the surface pressure (solid lines) and for the Laplace pressure (dashed lines) along isotherms 1 K and 24.57 K almost merge together on this scale.

Figure 2 from top to bottom shows isotherms $T = 100$, 500, 1000 K for BCC-Li ($T_m(P = 0) = 453.69$ K). Figure 2, *a* shows that the specific surface energy dependences $\sigma(v/v_0)$ along the three isotherms almost merge together in the fragmentation point on this scale. In Figure 2, *b*, all three dependence isotherms both for the surface pressure (solid lines) and for the Laplace pressure (dashed lines) for the nanocrystal consisting of 281 atoms merge together on this scale.

Figure 3 from top to bottom shows isotherms $T = 300$, 3000, 10000 K for FCC-Au crystal ($T_m(P = 0) = = 1337.58$ K). In Figure 3, *b*, all three dependence isotherms for the surface pressure (solid lines) for the nanocrystal consisting of 306 atoms merge together on this scale.

There are various estimates, both experimental and theoretical (in brackets), of $\sigma(100)$ for the macrocrystal with $P = 0$ in the literature:

$$\sigma(\text{Ne}),\ 10^{-3}\,\text{J/m}^2 = (12.7)\ (0\,\text{K})\ [22],$$

$$(15)\ (0\,\text{K}) - 12\ (T_m)\ [34],\ (17.9)\ (0\,\text{K})\ [35];$$

$$\sigma(\text{Li}),\ 10^{-3}\,\text{J/m}^2 = 472\ (T_m)\ [36],\ 522 - 525,\ (522)\ [37],$$

$$520 - 530,\ (520 - 580)\ [38],\quad (526)\ (0\,\text{K})\ [39];$$

$$\sigma(\text{Au}),\ 10^{-3}\,\text{J/m}^2 = 1410 \pm 37\ [7],$$

$$1500 - 1540\ (0\,\text{K}),\ 1333\ (T_m)\ [36],$$

$$1500 - 1506\ (1627)\ [37];$$

$$1500 - 1510\ (1630 - 1800)\ [38],$$

$$1363\ (T_m)\ [40],\ \ 1510 \pm 160\ (850 - 1710)\ [41].$$

Table 2 shows the following values calculated for macrocrystals at various temperatures: $\sigma(v/v_0 = 1)$ — specific surface energy of the (100) facet with $v/v_0 = 1$, $(v/v_0)_{max}$ and σ_{max} — normalized volume and specific surface energy in the maximum point of isotherm $\sigma(v/v_0)$, $(v/v_0)_{frS}$ — normalized volume in the fragmentation point.

The right column shows P_{frS} — experimental and theoretical (in brackets) pressure corresponding to $(v/v_0)_{frS}$.

As shown in Table 2, there is quite good agreement between our calculated values of $\sigma(v/v_0 = 1)$ and the experimental estimates at $P = 0$.

4. Discussion of the results

In [22], it was found that $\sigma(P)$ calculated for FCC-Ne along isotherm $T = 0$ K crosses zero at $P_{frS} = 2.8$ GPa. This agrees with the estimated pressure calculated in [45] for $(v/v_0)_{frS}$ as listed in Table 2. However, the experimental pressures from [44] for the specified value of $(v/v_0)_{frS}$ are much lower. For Li and Au, experimental and theoretical pressure estimates for the calculated $(v/v_0)_{frS}$ almost coincide. As shown in Table 2, pressures required for transition to the baric exothermic fragmentation region are quite attainable in the modern experiments [50,51]. However, the baric fragmentation process in Ne may go very slowly at low temperatures, in the 40−70 GPa region (region of the minimum on Li melting curve $T_m(P)$) in Li, several polymorphous phases [50] are observed, and for Au above 200 GPa, instability of the FCC structure is observed [51]. Is it related to the baric fragmentation? We cannot answer this question yet.

The process of transition from the metastable single-crystal state to the nanodispersed stable state at $P > P_{frS}$ obviously has a particular relaxation time. Therefore, the fragmentation will start not immediately after achievement

Table 2. Temperature, specific surface energy and normalized volume in the maximum point and fragmentation point, P_{frS} — pressure corresponding to $(v/v_0)_{\text{frS}}$

Crystal, $T_m(P=0)$, K	T, K	$\sigma(v/v_0=1)$, 10^{-3} J/m^2	$(v/v_0)_{\max}$	$\sigma_{\max}$, 10^{-3} J/m^2	$(v/v_0)_{\text{frS}}$	P_{frS}, GPa
FCC-Ne 24.57	1	8.14894	0.9820	8.1764	0.7906	0.65 [42], (3.3–3.5) [43]
	24.57	7.91278	0.9734	7.9677	0.7909	–
	300	−1.9355	0.9519	−1.7688	Point is missing	–
BCC-Li 453.69	100	590.398	0.6777	686.85	0.3809	50–55 [44], (56–60) [45]
	500	574.242	0.6787	668.64	0.3828	–
	1000	552.017	0.6846	640.32	0.3874	–
FCC-Au 1337.58	300	1556.43	0.9082	1613.20	0.6710	200.5 [46], (170–205) [47], 210 [48], 180–205 [49]
	3000	1414.55	0.9144	1462.52	0.6791	199.0 [46], (165–200) [47], 213 [48]
	10000	1045.94	0.9308	1073.55	0.7050	–

of P_{frS}, but the probability of crystal fragmentation (as all processes accompanying this effect) will increase as $P-P_{\text{frS}}$ grows and also as the system holding time increases at this pressure.

In [3–6], fragmentation was observed in dynamic shear deformation of crystals. Fragmentation was assumed as crystal transfer into an unstable nanodispersed state. This was due to the fact that crack healing takes place during further annealing of the samples. However, as shown in this work, single crystal is unstable with $P > P_{\text{frS}}$. Therefore, its transition to the stable nanodispersed state shall be accompanied by heat release at $P > P_{\text{frS}}$. Unfortunately, this exothermic effect hasn't been experimentally studied yet.

For experimental validation of our baric fragmentation theory, focus may be made on a bimodal domain size distribution effect that was found in [52] during investigation of megaplastic deformation in a Fe-Ni alloy (solid solution with FCC structure). Similar bimodal domain size distribution in megaplastic deformation was later also found in other metals [6]. Domain size distribution bimodality was also detected in [53] in megaplastic deformation of BCC-Nb. As long as during fragmentation $\sigma < 0$, then it is favorable for the nanocrystal to have the largest surface area. Therefore, at $P > P_{\text{frS}}$, the „non-cubic" forms ($f \neq 1$) of nanocrystal are energetically more favorable that the cubic form ($f = 1$) for the same isomers. As can be seen from (7), two values $f \neq 1$ correspond to a certain value of $Z_s(f \neq 1)$ for the RP model: for plate (where $f_p < 1$) and for rod (where $f_r > 1$). For these two shape parameters, the following is satisfied: $Z_s(f_p < 1) = Z_s(f_r > 1)$. Hence, it follows that at constant k_p, and T and $P > P_{\text{frS}}$, there are two energetically equal forms of nanocrystal: plate-like ($f_p < 1$) and rod-like ($f_r > 1$), that have different geometric sizes. This explains the bimodal domain size distribution obtained in [52,53]. From these considerations, it can be also easily understood why detonation diamonds grown from carbon have a flattened or needle-like shape [54]. Note that the „non-cubic" nanocrystal bimodality within the RP model was predicted in 2004 in [11].

Note that formalism (2)–(16) didn't consider the presence of either diffusing atoms or vacant lattice sites in the crystal. This was due to the fact that, as shown in [31,55–57], consideration of these activation processes affects the crystal properties only at $v/v_0 > 1$. With $v/v_0 < (v/v_0)_{\max}$, the effect of these activation processes on the crystal properties is negligible. Therefore, when calculating the equation of state and crystal surface properties at $v/v_0 < (v/v_0)_{\max}$ didn't consider these activation processes. However, the fragmentation increases the interdomain surface area, thus, increasing the atom migration over the interdomain surface. As shown in [58,59], domain boundary diffusion has an activation energy that is much lower than that within a single crystal. Therefore, the self-diffusion coefficient for crystal transition to the nanodispersed state in such medium will be much higher than in a single crystal. Anomalously high self-diffusion of atoms in crystal fragmentation was shown experimentally in [5,6].

In [60], it was shown experimentally that „after severe plastic deformation, the boundaries of W and Mo ultrafine grains (mean crystallite size was $\sim 200-300$ nm) were in non-equilibrium state that featured excess free volume. During annealing, the grain boundary state changes and approaches the state typical of coarse-grained materials". In [61], it was shown experimentally that grain boundaries in severe plastic deformation of the Ti_2NiCu crystalline alloy changed to amorphous state, expanded and were transformed into a bulk amorphous phase. It can be easily understood that a baric-fragmented „ultra-fine grain" or X-ray amorphous state of metal at $P > P_{\text{frS}}$ is more stable

than a single-crystal state. However, when $P < P_{frS}$, these states are less stable and, therefore, will change to a single-crystal state during annealing. It is obvious that for this a certain relaxation time is needed and will be shorter with higher annealing temperature of this non-equilibrium states at $P < P_{frS}$ [62]. In such transition from non-equilibrium to single-crystal state, energy shall be released due to amorphous phase crystallization and decrease in the internal metal surface.

5. Conclusion

The RP model showed that, at certain normalized volume: $(v/v_0)_{frS} < (v/v_0)_{max} < 1$, the specific surface energy of crystal moves to the negative region. It was shown that such behavior of $\sigma(v/v_0)$ at $v/v_0 < (v/v_0)_{frS}$ shall induce fragmentation where the crystal will tend to increase its specific (per atom) intercrystalline surface in any way.

It is shown that at $v/v_0 < (v/v_0)_{frS}$ the negative value of $\sigma(v/v_0)$ shall stimulate both crystal structure fragmentation and heating of fragmenting medium, and occurrence of additional surface pressure P_{sf} in this medium. P_{sf} increases as the „average“ nanocrystal size over the medium decreases, as the nanocrystal shape differs more significantly from the energetically optimum shape at $P < P_{frS}$ (this is cube for the RP model) and as the external pressure increases. Additional all-round pressure P_{sf} will cause a decrease in the compression modulus both for an individual nanocrystal and for the whole fragmenting medium.

The values of $(v/v_0)_{max}$ and $(v/v_0)_{frS}$ were calculated for Ne, Li and Au crystals at various temperatures. Experimental data ware used to specify pressures corresponding to these values of $(v/v_0)_{frS}$.

Thus, the following answers may be given to the questions posed in the introduction. In all-round compression above a certain P_{frS}, the crystal fragments into domains and increases its internal interdomain surface due to transition of the specific surface energy with $P > P_{frS}$ to the negative value region. Temperature has a little effect on $(v/v_0)_{frS}$ or P_{frS}. When the crystal changes from the single-crystal to nanodispersed state, additional surface pressure P_{sf} occurs and affects both the equation of nanodispersed crystal state and the isothermal modulus of elasticity of the dispersive medium.

Acknowledgments

The author is grateful to S.P. Kramynin, K.N. Magomedov, N.Sh. Gazanova, Z.M. Surkhayeva and M.M. Gadzhieva for fruitful discussions and assistance in work.

Funding

This study was supported by the grant provided by the Russian Science Foundation No. 25-23-00001, https://rscf.ru/project/25-23-00001/.

Conflict of interest

The author declares that he has no conflict of interest.

References

[1] C.C. Zurkowski, J. Yang, F. Miozzi, S. Vitale, E.F. O'Bannon III, Z. Jenei, S. Chariton, V. Prakapenka, Y. Fei. Sci. Rep. **14**, *1*, 11412 (2024). https://doi.org/10.1038/s41598-024-61861-2
[2] P.W. Bridgman. Studies in large plastic flow and fracture: with special emphasis on the effects of hydrostatic pressure. Harvard University Press, Cambridge, Massachusetts (1964). 363 p. https://doi.org/10.4159/harvard.9780674731349
[3] S. Leoni, R. Ramlau, K. Meier, M. Schmidt, U. Schwarz. PNAS **105**, *50*, 19612 (2008). https://doi.org/10.1073/pnas.0805235105
[4] T.M. Gapontseva, M.V. Degtyarev, V.P. Pilyugin, T.I. Chashchukhina, L.M. Voronova, A.M. Patselov. Phys. Metals. Metallogr. **117**, *4*, 336 (2016). https://doi.org/10.1134/S0031918X16040062
[5] Y. Cao, S. Ni, X. Liao, M. Song, Y. Zhu. Mater. Sci. Eng.: R: Reports **133**, 1 (2018). https://doi.org/10.1016/j.mser.2018.06.001
[6] A.M. Glezer, R.V. Sundeev, A.V. Shalimova, L.S. Metlov. Phys.−Uspekhi **66**, *1*, 32 (2023). https://doi.org/10.3367/UFNe.2021.07.039024
[7] V.K. Kumikov, Kh.B. Khokonov. Appl. Phys. **54**, *3*, 1346 (1983). https://doi.org/10.1063/1.332209
[8] S.N. Zhevnenko, I.S. Petrov, D. Scheiber, V.I. Razumovskiy. Acta Materialia **205**, 116565 (2021). https://doi.org/10.1016/j.actamat.2020.116565
[9] S. Zhu, K. Xie, Q. Lin, R. Cao, F. Qiu. Adv. Colloid. Interface Sci. **315**, 102905 (2023). https://doi.org/10.1016/j.cis.2023.102905
[10] M.N. Magomedov. Phys. Rev. B **109**, *3*, 035405 (2024). https://doi.org/10.1103/PhysRevB.109.035405
[11] M.N. Magomedov. Phys. Solid State **46**, *5*, 954 (2004). https://doi.org/10.1134/1.1744976
[12] M.N. Magomedov. Crystallogr. Rep. **62**, *3*, 480 (2017). https://doi.org/10.1134/S1063774517030142
[13] M.N. Magomedov. Phys. Solid State **63**, *10*, 1465 (2021). https://doi.org/10.1134/S1063783421090250
[14] M.N. Magomedov. Phys. Solid State **66**, *3*, 428 (2024).
[15] M.N. Magomedov. Tech. Phys. **58**, *9*, 1297 (2013). https://doi.org/10.1134/S106378421309020X
[16] M.N. Magomedov. Tech. Phys. **55**, *9*, 1382 (2010). https://doi.org/10.1134/S1063784210090240
[17] M.N. Magomedov. Phys. Solid State **62**, *12*, 2280 (2020). https://doi.org/10.1134/S1063783420120197
[18] S.P. Kramynin. J. Phys. Chem. Solids **143**, 109464 (2020). https://doi.org/10.1016/j.jpcs.2020.109464
[19] S.P. Kramynin. J. Phys. Chem. Solids **152**, 109964 (2021). https://doi.org/10.1016/j.jpcs.2021.109964
[20] S.P. Kramynin. Phys. Metals. Metallogr. **123**, *2*, 107 (2022). https://doi.org/10.1134/S0031918X22020065
[21] S.P. Kramynin. Solid State Sci. **124**, 106814 (2022). https://doi.org/10.1016/j.solidstatesciences.2022.106814
[22] A.K. Kyarov, A.I. Temrokov, B.V. Khaev. High Temperature **35**, *3*, 380 (1997).

[23] M.N. Magomedov. J. Surface Investigation. X-ray, Synchrotron. Neutron Technique **6**, *3*, 430 (2012). https://doi.org/10.1134/S1027451012050151
[24] M.N. Magomedov. J. Surface Investigation. X-ray, Synchrotron. Neutron Techniques **7**, *6*, 1114 (2013). https://doi.org/10.1134/S1027451013060104
[25] M.N. Magomedov. Tech. Phys. **61**, *5*, 722 (2016). https://doi.org/10.1134/S1063784216050145
[26] D.E. Grady. J. Mech. Phys. Solids **36**, *3*, 353 (1988). https://doi.org/10.1016/0022-5096(88)90015-4
[27] N. Amadou, T. de Rességuier. Phys. Rev. B **108**, *17*, 174109 (2023). https://doi.org/10.1103/PhysRevB.108.174109
[28] Y.Kh. Vekilov, O.M. Krasilnikov. Phys.−Uspekhi **52**, *8*, 831 (2009). https://doi.org/10.3367/UFNe.0179.200908f.0883.
[29] L. Bellino, G. Florio, S. Giordano, G. Puglisi. Applications in Engineering Science **2**, 100009 (2020). https://doi.org/10.1016/j.apples.2020.100009
[30] M.N. Magomedov. High Temperature **44**, *4*, 513 (2006). https://doi.org/10.1007/s10740-006-0064-5
[31] M.N. Magomedov. J. Surface Investigation. X-ray, Synchrotron and Neutron Techniques **7**, *4*, 697 (2013). https://doi.org/10.1134/S1027451013030087
[32] M.N. Magomedov. High Temperature **47**, *2*, 219 (2009). https://doi.org/10.1134/S0018151X09020114
[33] M.N. Magomedov. Phys. Solid State **64**, *7*, 765 (2022). https://doi.org/10.21883/PSS.2022.07.54579.319
[34] R.E. Allen, F.W. De Wette. J. Chem. Phys. **51**, *11*, 4820 (1969). https://doi.org/10.1063/1.1671873
[35] R. Shuttleworth. Proceed. Phys. Soc. Section A **63**, *5*, 444 (1950). https://doi.org/10.1088/0370-1298/63/5/302
[36] W.R. Tyson, W.A. Miller. Surf. Sci. **62**, *1*, 267 (1977). https://doi.org/10.1016/0039-6028(77)90442-3
[37] L. Vitos, A.V. Ruban, H.L. Skriver, J. Kollár. Surface Sci. **411**, *1−2*, 186 (1998). https://doi.org/10.1016/s0039-6028(98)00363-x
[38] Q. Jiang, H.M. Lu, M. Zhao. J. Phys.: Condens. Matter **16**, *4*, 521 (2004). https://doi.org/10.1088/0953-8984/16/4/001
[39] B. Fu, W. Liu, Z. Li. Mater. Chem. Phys. **123**, *2−3*, 658 (2010). https://doi.org/10.1016/j.matchemphys.2010.05.034
[40] B.B. Alchagirov, T.M. Taova, Kh.B. Khokonov. Trans. JWRI. Special Issue (Japan) **30**, 287 (2001). https://repository.exst.jaxa.jp/dspace/handle/a-is/48071
[41] A. Patra, J.E. Bates, J. Sun, J.P. Perdew. PNAS **114**, *44*, E9188 (2017). https://doi.org/10.1073/pnas.1713320114
[42] M.S. Anderson, R.Q. Fugate, C.A. Swenson. J. Low Temperature Phys. **10**, *3−4*, 345 (1973). https://doi.org/10.1007/BF00654913
[43] A. Mishra, K. Dharmendra. J. Phys.: Conf. Ser. **2007**, *1*, 012007 (2021). https://doi.org/10.1088/1742-6596/2007/1/012007
[44] C.L. Guillaume, E. Gregoryanz, O. Degtyareva, M.I. McMahon, M. Hanfland, S. Evans, M. Guthrie, S.V. Sinogeikin, H.-K. Mao. Nature Phys. **7**, *3*, 211 (2011). https://doi.org/10.1038/NPHYS1864
[45] S.V. Chernov. High Temperature **26**, *2*, 191 (1988).
[46] D.L. Heinz, R. Jeanloz. J. Appl. Phys. **55**, *4*, 885 (1984). https://doi.org/10.1063/1.333139
[47] C.-H. Nie, L.-R. Chen. Physica Status Solidi (b) **215**, *2*, 957 (1999). https://doi.org/10.1002/(sici)1521-3951(199910)215:2¡957::aid-pssb957¿3.0.co;2-q
[48] M. Yokoo, N. Kawai, K.G. Nakamura, K. Kondo, Y. Tange, T. Tsuchiya. Phys. Rev. B **80**, *10*, 104114 (2009). https://doi.org/10.1103/PhysRevB.80.104114
[49] S.M. Dorfman, V.B. Prakapenka, Y. Meng, T.S. Duffy. J. Geophys. Res.: Solid Earth **117**, *B8*, B08210 (2012). https://doi.org/10.1029/2012JB009292
[50] X. Wang, Z. Wang, P. Gao, C. Zhang, J. Lv, H. Wang, H. Liu, Y. Wang, Y. Ma. Nature Commun. **14**, *1*, 2924 (2023). https://doi.org/10.1038/s41467-023-38650-y
[51] P. Richard, A. Castellano, R. Béjaud, L. Baguet, J. Bouchet, G. Geneste, F. Bottin. Phys. Rev. Lett. **131**, *20*, 206101 (2023). https://doi.org/10.1103/PhysRevLett.131.206101
[52] A.M. Glezer, V.N. Varyukhin, A.A. Tomchuk, N.A. Maleeva. Doklady Phys. **59**, *8*, 360 (2014). https://doi.org/10.1134/S1028335814080059
[53] V.V. Popov, E.N. Popova. Mater. Trans **60**, *7*, 1209 (2019). https://doi.org/10.2320/matertrans.MF201913
[54] A.N. Ozerin, T.S. Kurkin, L.A. Ozerina, V.Yu. Dolmatov. Crystallogr. Rep. **53**, *1*, 60 (2008). https://doi.org/10.1134/S1063774508010070
[55] M.N. Magomedov. Phys. Metals. Metallogr. **114**, *3*, 207 (2013). https://doi.org/10.1134/S0031918X13030113
[56] M.N. Magomedov. Tech. Phys. **58**, *12*, 1789 (2013). https://doi.org/10.1134/S1063784213120153
[57] M.N. Magomedov. Tech. Phys. **68**, *2*, 209 (2023). https://doi.org/10.21883/TP.2023.02.55474.190-22
[58] R.K. Koju, Y. Mishin. Nanomater. **11**, *9*, 2348 (2021). https://doi.org/10.3390/nano11092348
[59] V.V. Popov, E.V. Osinnikova, A.Yu. Istomina, E.N. Popova, R.M. Falakhutdinov. Phys. Metals. Metallogr. **124**, *6*, 561 (2023). https://doi.org/10.1134/S0031918X23600781
[60] V.V. Popov, A.V. Sergeev, A.V. Stolbovsky. Phys. Metals. Metallogr. **118**, *4*, 354 (2017). https://doi.org/10.1134/S0031918X17040081
[61] R.V. Sundeev, A.V. Shalimova, A.M. Glezer, E.A. Pechina, M.V. Gorshenkov, G.I. Nosova. Mater. Sci. Eng.: A **679**, 1 (2017). https://doi.org/10.1016/j.msea.2016.10.028
[62] D.Y. Kovalev, I.I. Chuev. Tech. Phys. **65**, *10*, 1652 (2020). https://doi.org/10.1134/S1063784220100102

Translated by E.Ilinskaya